Opto-Electronic Advances

Review

2018, Vol. 1, No. 4

DOI: 10.29026/oea.2018.180008

Fabrication of three-dimensional proteinaceous micro- and nano-structures by femtosecond laser cross-linking

Daniela Serien, Koji Sugioka*

Proteins are a class of biomaterials having a vast array of functions, including the catalysis of metabolic reactions, DNA replication, stimuli response and transportation of molecules. Recent progress in laser-based fabrication technologies has enabled the formation of three-dimensional (3D) proteinaceous micro- and nano-structures by femtosecond laser cross-linking, which has expanded the possible applications of proteins. This article reviews the current knowledge and recent advancements in the femtosecond laser cross-linking of proteins. An overview of previous studies related to fabrication using a variety of proteins and detailed discussions of the associated mechanisms are provided. In addition, advances and applications utilizing specific protein functions are introduced. This review thus provides a valuable summary of the 3D micro- and nano-fabrication of proteins for biological and medical applications.

Keywords: laser direct write; femtosecond laser; cross-linking; protein; 3D fabrication; microfluidics; actuation; scaffold

Serien D, Sugioka K. Fabrication of three-dimensional proteinaceous micro- and nano-structures by femtosecond laser cross-linking. *Opto-Electronic Advances* **1**, 180008 (2018).

Introduction

Amongst the three groups of essential biomaterials, fats, sugars and proteins, proteins are the most vital in cell development, cell-to-cell communication and cellular sensing[1,2]. As such, the selective binding of proteins is an attractive means of performing various analytical tests and of achieving targeted drug delivery. Furthermore, the formation of three-dimensional (3D) protein microenvironments that can control or influence cellular growth and development is currently of significant interest in the field of tissue engineering.

Based on *in situ* gelation processes, protein hydrogels have been fabricated by solvent exchange, ultraviolet (UV) irradiation, ionic cross-linking, pH changes and temperature modulation[3]. The use of enzymes can also create artificial, cross-linked hydrogels with free enzyme[4], localized[5] or self-assembled structures[6]. These methods allow the formation of complex nano-scale protein hydrogel structures with high-throughput in a controlled manner[4]. Cell-laden cross-linking using a photoinitiator in conjunction with UV exposure can lead to cytotoxicity, while physical cross-linking results in lower mechanical stability compared to a covalently bonded hydrogel[4]. Nevertheless, because the cross-linking density, resulting mechanical properties and applicable residues are all well controlled by these methods, microfluidic mixers[7,8], drug delivery colloids[9] and rare element mining[10] are promising applications, in addition to cell culturing for tissue engineering and regenerative medicine[4,8]. These techniques can produce large quantities of structures at reasonable speeds, although it is challenging to establish suitable microenvironments for biological studies.

Since microfluidic devices can create shell-and-core streams (so-called laminar flow) in microchannels, shell-and-core fibers containing protein and matrix material are fabricated at desired diameter and length[11]. Cells can be suspended into a desired stream and grown inside the specific environment[11]. Dissolvable materials grown in the outer shell can be used to support handling and transport of these fibers as well as to prevent bacterial infection[11]. Cellular structures that prefer elongated environments are more readily obtained using such configurations[12,13]. However, limited growth space and difficulty in the spatial patterning of cells in the case of certain flow processes represent current challenges associated with this technology.

Rather than using laminar flow to shape a microenvironment, proteinaceous microspheres can be obtained from water-in-oil emulsions[14] or by high-intensity ultrasound[15]. The size distribution and dispersion of these

Advanced Laser Processing Research Team, RIKEN Center for Advanced Photonics, 2-1 Hirosawa, Wako, Saitama 351-0198, Japan
* Correspondence: K Sugioka, E-mail: ksugioka@riken.jp
Received 10 May 2018; accepted 6 June 2018; accepted article preview online 7 June 2018

microspheres can be fine-tuned by varying certain parameters and additives[14]. In the case of the ultrasound method, either air of liquids other than water can be employed[15]. In addition, because proteins are not significantly denatured within nanometer-sized shells[15], these microspheres can be applied to wound healing in association with appropriate oils[16]. In another application, microbubbles filled with sonographic contrast agents were applied to contrast-specific imaging in animals based on non-linear optical interactions[17]. Fabrication by emulsion or ultrasound allows processing that is both rapid and large-scale, although the resulting spherical structure size distributions are limited.

In order to mimic the complexity of biological systems using artificial proteinaceous structures, a more diverse selection of protein microenvironments is required, along with increased spatial resolution. Ink jet printing based on gel droplets has been utilized to obtain improved spatial control, 3D fabrication capabilities and the ability to create multi-material and multi-cellular hydrogels[18]. Although this process involves the release of cell-laden or bare protein matrix droplets and is time consuming, it permits the engineering of complex microenvironments within a given volume[19,20]. Using sacrificial materials, it is also possible to create hollow features, such as vascularized tissues[21]. The extent of spatial control is, however, limited to the nozzle aperture size and can also be restricted by the associated gelation processes, such that the typical fabrication resolution is currently several tens of μm. Additionally, soft structures obtained using this method are often difficult to move or handle during subsequent processing or cell culture analysis steps.

Using laser light as a propulsion source, proteins and cells can be transferred from a thin-film biomaterial deposited on a transparent donor substrate to the surface of an accepter substrate[22]. This process is termed laser-induced forward transfer (LIFT). Modulating the impact strength and the number of stacked layers can produce thick 2D structures, and even 3D structures become feasible by the use of sacrificial materials. Similar to an inkjet process, this transfer method requires no contact by the fabrication device and so the fluid properties are not a primary factor. Unfortunately, the requirement to propel the film material to another surface limits throughput, since the layer thickness achieved by a single laser shot is limited to several hundreds of nanometers[23]. Thicker cell-laden hydrogel layers have been patterned by taking advantage of the thermal expansion of a polyimide donor plate or based on absorption by a metal layer formed between the biomaterial thin film and the donor substrate [24,25]. Although the resolution of this method (at approximately several μm) is superior to that obtained using an inkjet process, the formation of complex 3D structures is difficult.

Recently, the photo-induced cross-linking of proteins using laser direct writing has attracted much attention as an alternative means of producing 3D proteinaceous micro- and nano-structures with high resolution. Figure 1 shows a general setup and a schematic description of the fabrication of proteinaceous microstructures and will be discussed in greater detail later. In such processes, solutions containing mixtures of proteins and photoinitiators (or photosensitizers) are used as precursors[26]. The multiphoton cross-linking of proteins is similar to multiphoton polymerization using photocurable resins or negative-tone resists. This mechanism has also been employed for the cross-linking of DNA for cell analysis[27,28]. Utilizing a femtosecond (fs) laser multi-photon technique has further enabled the creation of complex 3D structures[29,30]. In multi-photon cross-linking, multiple spatiotemporally coincident longer wavelength photons generate an absorption scheme equivalent to that of a single photon having a shorter wavelength, in a process known as multiphoton absorption. As a result, electrons in materials can be excited solely at a focal volume of incident laser light, at which photon intensity exceeds the threshold intensity to substantially satisfy the probability of multiphoton absorption. Thus, photo-induced cross-linking can be confined to the focal volume. Furthermore, since the beam profile is Gaussian and the probability of multiphoton absorption is proportional to the laser intensity raised to the power of n, where n is the number of photons absorbed, the effective spot size will be smaller by the factor $1/n^{1/2}$ than the spot size for single photon absorption[30,31], enabling spatially localized cross-linking with higher resolution.

Based on the absorption properties of the precursor solution (the mixture of proteins and a photoinitiator or photosensitizer), an appropriate femtosecond laser wavelength must be selected to restrict the solidification process solely to the focal volume during the multi-photon process[32]. The non-invasive nature of forming cross-linked proteins in solution enables the fabrication of various complex embedded 3D structures. These structures can be nested on the substrate surfaces[33,34] or embedded into transparent devices such as microfluidic channels[35–37].

In addition to 3D fabrication and superior resolution, another advantage of the multi-photon cross-linking of proteins as 3D printing materials is the potential to retain the protein functions after fabrication[35,38,39]. These functions include not only the diverse intrinsic properties of native proteins such as charge transfer, molecule modification and cell-cell communication, but also engineered functions of synthetic proteins. Consequently, the resulting protein structures have been applied to fabricate functional microdevices, including pH-sensitive actuators[39,40] and optical microcomponents[41,42]. The integration of proteinaceous microstructures into commercial polymers[43] and protein-polymer hybrids[44] has also been found to increase mechanical strength.

This review article presents a comprehensive summary

of the current understanding and recent advancements in the femtosecond laser cross-linking of 3D proteinaceous micro- and nano-structures. Protein types and fabrication conditions employed in previous works are summarized, and the possible mechanisms associated with this technique as well as the properties of the treated proteins are discussed. Advances, present-day applications and the potential for future applications are also described. Due to the abundance of native, modified and synthetic proteins with various functions, we believe that the femtosecond laser cross-linking of proteinaceous microstructures offers numerous applications in biological studies, lab-on-a-chip and total analysis systems.

Survey of previous research

Table 1 summarizes the studies reported to date regarding femtosecond laser cross-linking in terms of the protein solutions employed, while Table 2 presents the laser fabrication conditions. In this section, both fabrication conditions and the properties of the resulting cross-linked proteins are discussed.

Fabrication conditions

Lasers and direct writing systems

In order to initiate cross-linking, a laser beam is applied to a precursor material. The beam path can be guided and shaped in various ways, and the overall system includes at least three basic components as shown in Fig. 1a: a laser, a lens and mirror system to direct and (optionally) shape the light, and an objective lens to focus the laser beam on the sample.

The laser beam, typically a linearly polarized Gaussian beam, is expanded by a collimation system to match the back-end aperture of the objective lens. Static mirrors are the simplest optical element used to guide the laser beam towards the sample. The average power of the laser can be controlled by rotating a half waveplate placed in front of a polarizer. If the combination of the half waveplate and the polarizer does not allow sufficient attenuation of the femtosecond laser pulses because of the limited extinction ratio, additional neutral density filters can be inserted after the polarizer to obtain a broader tunable range. The laser beam focused by the objective lens subsequently irradiates the sample in either an upright or inverted configuration.

In most patterning systems, a mechanical or piezo stage is used to move the sample during the laser irradiation. Such scanning stage systems cover wide areas to precisely move the samples in 3D, but the fabrication efficiency is limited by the scanning speed of stages. Another issue is residual vibration from movements. Alternatively, a dynamic mirror such as a galvano mirror can be used, which rapidly scans the laser beam across, while the scanning area is limited as a result of small angular changes. Galvano mirror scanning is popular in polymer fabrication because the high photosensitivity of these materials requires the avoidance of prolonged exposure to the beam. Combination of the scanning mirror and stage can be used for rapid volume fabrication.

As another alternative, a spatial light modulator (SLM) can be employed to control the light amplitude and phase to spatially shape the laser beam for multi-focal patterning or single-shot pattern projection[34,39,47,57,58,60,64,65]. Light modulation is achieved either by a digital mirror device (DMD) composed of an array of individually rotatable micro-mirrors, or a liquid crystal display (LCD) composed of an array of individual liquid crystal pixels electrically modulating the light. Light modulation is limited by the loss of light intensity resulting from interferences of individual lights modulated in amplitude or phase when shaping the light into the desired pattern. Single spot projection patterning with SLM is a maskless technology that allows flexible shaping of the amplitude in space and thus permits dynamic lithography. Direct writing is a slow process because the patterning is performed by scanning with a focused laser spot, while multi-focal patterning or pattern projection using SLM can enhance the throughput of laser direct writing.

Typically, a high numerical aperture (*NA*) objective lens, in particular a 100× water or oil immersion lens with *NA*=1.3–1.4, is used to focus the beam at the precursor material. In Table 2, feature sizes were obtained by using these high-*NA* objective lenses. In principle, the feature sizes of fabricated elements are determined by the spot size obtained by focusing with the objective lens. The full width at half maximum (FWHM) size of the focal spot (which represents the diffraction limit) in the lateral direction (plane perpendicular to the laser beam axis) is given by $1.22\lambda/NA$, where λ is the laser wavelength. Employing the objective lens with *NA*=1.4, the focal spot size can be calculated to be ca. 700 nm for the wavelength of 800 nm. The feature sizes obtained using multi-photon cross-linking can be less than the focal spot size of the focused laser due to the Gaussian beam profile of the laser beam and the fabrication threshold for the process[31], as shown schematically in Fig. 1a. Theoretically, the feature sizes can be decreased without no limitation by setting the laser intensity at the center of laser beam to the fabrication threshold as much as possible. However, in practice, around 200 nm is the minimum size due to pulse-to-pulse fluctuation of laser energy and instability of the scanning system as summarized in Table 2. Figure 1b shows that feature sizes in volume are determined by the laser writing scheme. In a free space, features of voxel becomes ellipsoidal shapes due to mismatch between focused spot sizes and Rayleigh lengths. On the substrate, surface bound structures are formed, as indicated by solid and dashed lines, depending on the position of focus. Determining resolution as the smallest distance between distinguishable structures, well-connected 3D structures can be formed by scanning the focused laser beam with a step smaller than the resolution.

Table 1 | Protein solution conditions. A summary of previous fabrication conditions, focusing on protein and photosensitizer concentrations. Examples of typical solvents and protein databank samples are included. Photoactivator abbreviations: rose bengal (RB), methylene blue (MB), flavin mononucleotide (FMN), flavin dinucleotide (FAD), rhodamine B (RhB), rhodamine 6 G (R6G), benzophenone dimer (BPD), sodium 4-[2-(4-morpholino)benzoyl-2-dimethylamino]butylbenzenesulfonate (MBS). Solvent abbreviations are: dimethyl sulfoxide (DMSO), phosphate-buffered saline (PBS), 4-(2-hydroxyethyl)-1-piperazineethanesulfonic acid (HEPES).

Representative PDB code	Protein (mg/mL)		Photoactivator (mM)		Solvent	References
1B8J	Alkaline phosphatase (AP)	280–350, 9800, 2100	RB	0.25	Ascorbic acid (1 mM)	38
	AP-BSA					38, 32
1JV5	Antibody anti-A	n.a.	Eosin-Y	0.3	n.a.	35
1VYO	Avidin	50–400	FMN, FAD, MB, RB	0, 1.2–8.5	Distilled water or buffer (PBS or HEPES), pH ~7.4	39, 45–49
			Eosin-Y, MB	14.3, 4.3	DMSO 21% in HEPES buffer	34
			FAD with RhB	0.250 with 0.407	12.5% HEPES, 19% DMSO, organic solvents	43
4F5S	Bovine serum albumin (BSA)	50–600, 800–1000[53]	Eosin-Y, Texas-Red, RhB, MBS, R6G, BPD, RB, FMN, FAD, MB	0–100	Distilled water or buffer (PBS or HEPES), pH ~7.3–4	32, 35, 37, 39, 41–42, 44–61
		210–460	Eosin-Y, MB, RB, RhB with FAD	4–14.3, 0.3–0.6 with 0.25	18%–23% DMSO in HEPES buffer (organic solvent)	34, 40, 43, 62–63, 66
		0–200	FAD, Benzophenone-biotin	0–2, 3–22	50% DMSO in buffer	33, 64
		100, 200	MBS	67–100	50%wt glycerol-water	37
	Biotinylated BSA (b-BSA)	100–300	FMN, FAD	1–5	Buffer (PBS or HEPES, pH ~7.4)	48, 61
	BSA conjugated with dye (dye-BSA)	200–400	RB, MB	0, 0.25, 5	Acetic or buffer, pH~7.3–4	38, 48, 58, 65
3HQV	Collagen type-I (Col.I)	15, 30, 45	FMN	0.6, 1.2, 1.8	Acetic acid, aqueous	67
	Collagen type-I, II, or IV (Col.I, Col.II, Col.IV)	2–3	BPD, RB	0.2, 1	Acetic acid, aqueous	52
1M3D	Col.IV - BSA	0.15, 25	FAD with RhB	0.125 with 0.3	As purchased (pH=5) mixed DMSO, HEPES buffer, organic solvent	43,66
1GKB	ConcanavalinA (ConA)	4.5	RB, Texas-red, RhB	0.5	n.a.	69
1OCC	Cytochrome c (CytC)	100, 200	FAD	0, 4.5, 10	Supporting electrolyte, pH=7.40.	46, 49, 68
2Y0G	Enhanced green fluorescent protein (EGFP)	2.35	MBS	10	HEPES-KOH buffer, pH = 7.4	37
3GHG	Fibrinogen (FNG)	3.9 or as purchased	RB, Texas-red, RhB	0.01–0.1	As purchased	32, 69
3M7P	Fibronectin (FN)	1–1.29	RB, Texas-red, RhB	2–4	Distilled water	44, 59, 69
2CMM	Myoglobin (MGN)	40	RB, MB	8.5 or 5	HEPES buffer (pH 7.4)	47
5IK4	Laminin (LN) mixed with BSA	n.a.	FAD, MB	1–4, 0.25	HEPES buffer (pH 7.4)	56
2CDS	Lysozyme (Lys)	300–400	MB, FAD	1.2–5	HEPES buffer (pH 7.4)	45, 47
		320–400	Eosin-Y, FAD, MB	4.3–14.3	DMSO 21%, HEPES buffer	34, 39
3UA0	Regenerated silk fibroin (RSF)	25	MB	5	Aqueous, pH=7.0	70
1S0Q	Trypsin (TR)	20	FAD, Eosin-Y	6, 0.3	n.a.	36

Table 2 | Laser fabrication conditions. Fabrication sorted by pulse width: femtosecond (fs), picosecond (ps) and nanosecond (ns). For almost all reports, high-*NA* lenses were used. BSA was employed for all conditions. Dynamic mirror device (DMD), spatial light modulator (SLM), or galvano mirrors were used in some of these previous works.

	Device	Pulse width	Frequency	Wavelength (nm)	Fabrication conditions	Special setups	Feature size	Protein	References
fs	Oscillator (Ti:Sa primarily)	<29 fs, 100–120 fs, 400 fs	54 MHz, 75 MHz, 76 MHz, 80 MHz, 82 MHz	525, 715, 740, 750, 780, 800, 806, 850	20–123 mW, 3.385-6.093 mW, 0.5–7 μm/s, corrected dose equivalent K_L: 0.01–100, 100–500 pJ/pulse, single spot 1 ms, 30–87 mW/μm^2		1 μm at 780 nm, 1.5 μm at 850 nm	BSA, RSF, FN, CytC, TR, Avidin, b-BSA, AP, BSA-AP, dye-BSA, Col.I, Col.II, Col.IV	36–38, 42, 44–45, 48, 50, 52, 55, 59, 61, 68–70
		100 fs, 120 fs	76 MHz, 80 MHz	740, 800	1.6 μs/pixel,120 mW, exposure doses 0–1.2 10^8 mJ/cm^2, 1000 μs/ 100 nm/20–40 mW, 24–66 mW/μm^2	galvano scan	200 nm	BSA, FNG, FN, ConA, AP, Avidin, CytC	32, 41, 46, 51, 53
		60 fs, <200 fs	76 MHz, 80 MHz	730–740, 750	5–105 mW, raster scan velocity of approx. 7 mm/s and a slow-axis velocity of 5–6 μm/s	DMD	submicron (0.5 μm)	BSA,dye-BSA, Avidin, Lys, MGN	34, 39, 47, 57-58, 60, 64
	Fiber	94 fs, 100–200 fs, 140 fs, 360 fs	200 kHz, 79.8-80 MHz	522, 740, 780, 790	0.09–144 mW, 0.2–10 μm/s, 30 μm/s, 70 μm/s, 2.4–9.1 nJ/μm^2 energy density		feature sizes > 250 nm, >150 nm	BSA, BSA/LN, Col.I, Col.IV, Avidin, EGFP	33, 37, 40, 43, 56, 62–63, 66, 67
ps (sub-ns)	Frequency-doubled μ-chip	550 ps	7 kHz	532	Corrected dose equivalent K_L: 0.01–100			BSA	44
	Diode-pumped Q-switched	800 ps, 600 ps	8 kHz, 7 kHz	532	Scanning up to 50 μm/s, 277–321 GW cm^{-2} peak, pulse E 3.5 μJ, 0.5–6 mW		140 nm (surface bound line)	BSA, CytC	48, 49
	Microlaser	500 ps	6.5 kHz, 40 kHz	532	15, 20, 40 mW, 5 μm/s, 0.15 mW of laser power and 1 ms exposure time			BSA,TR, anti-A antibody	35, 36, 50
ns	Q-switched solid state	12 ns	20 kHz	532	1 mW, 62 mW, 2–8 fps	SLM		BSA, dye-BSA	54, 65

Irradiation conditions

From Table 2, it is evident that various lasers have been employed for the cross-linking of proteins, including oscillator, mode-locked, Q-switched micro, solid state and fiber lasers. Q-switch lasers with picosecond pulses in the sub-nanosecond range are used for basic cross-linking, while femtosecond oscillators are utilized for microstructure fabrication. Longer pulse width causes heat generation and diffusion which induces irregularities such as spontaneous outbursts as well as thermal cross-linking, termed heat effect. Shorter pulse width is desirable because the heat effect can be minimized. Furthermore, most proteins have a denaturation temperature, at which their tertiary structure dissolves and function is lost. Therefore, shorter pulse width is preferred to ensure well-controlled fabrication quality and also prevent heat related protein denaturation. Both picosecond and femtosecond lasers create comparable feature sizes[45]. The femtosecond lasers available at present can be operated at considerably higher frequencies compared to picosecond lasers due to less heat accumulation effect, which increases the process speed. Picosecond lasers are affordable and compact, and thus also have applications in some fields. In addition, nanosecond lasers have been used for single shot cross-linking in conjunction with SLM-design holography[54,65]. The losses of light intensity resulting from complex interference patterns when using an SLM for 3D design requires can possibly be compensated for by heat associated with longer pulses, but it influences the cross-linking dynamics and quality of cross-linked proteins.

Near-infrared wavelengths are often elected because they are not absorbed by common photoinitiators such as rose bengal (RB) and methylene blue (MB), which is essential to inducing multi-photon absorption. Lasers with shorter pulse widths of approximately 100 fs are preferred in order to reduce any possible thermal effects, since both heat generation and cavitation bubbles in the aqueous environment can obstruct or degrade the fabrication process. When using mechanical or piezo stages, low laser energies in conjunction with high repetition rates with laser powers below 60 mW are adopted to reduce heat generation, while low scanning speeds on the order of μm/s are employed to allow sufficient time to induce cross-linking. Depending on the optional use of the

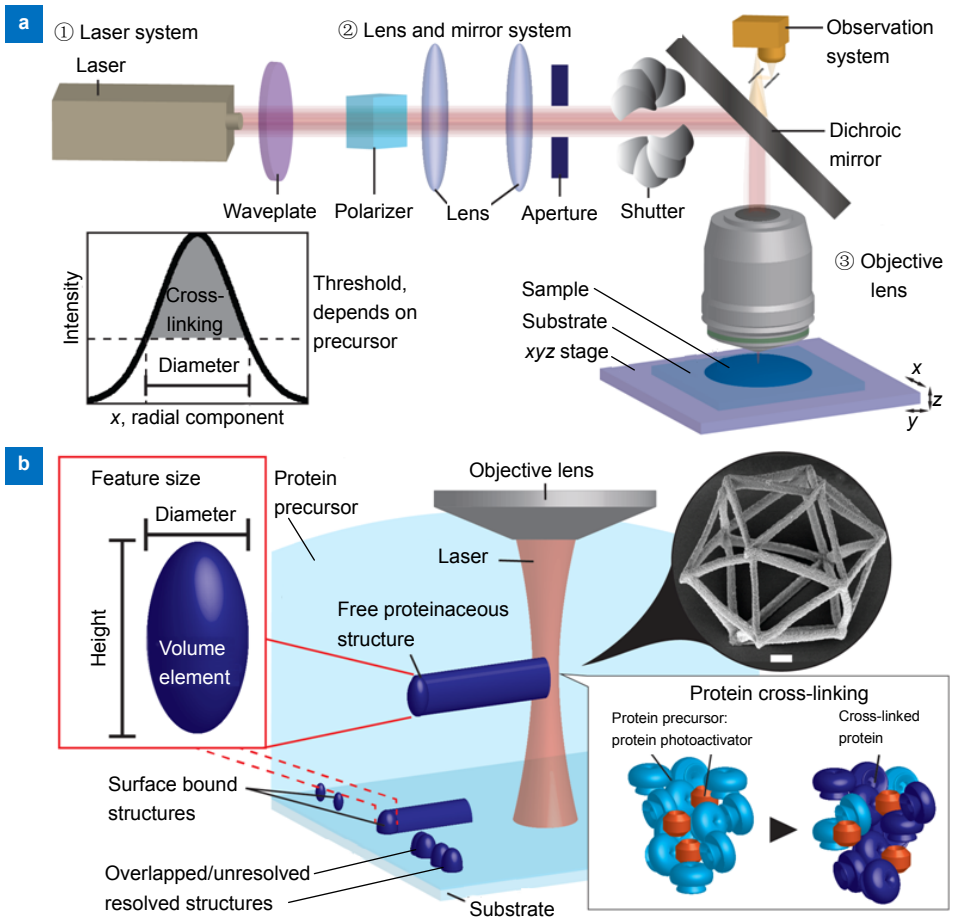

Fig. 1 | Laser writing system for microfabrication of proteinaceous structures. (**a**) Laser writing system is composed of three basic components: a laser, a lens and mirror system, and an objective lens. The beam is directed towards the sample mounted on a scanning stage, optionally observed with a white light camera setup. The system is controlled by a computer. The laser beam typically has a spatially Gaussian profile. In a plane perpendicular to the laser beam axis, the cross-linking occurs only in the beam where the intensity exceeds a threshold that is dependent on wavelength, absorption scheme (single or multiphoton absorption) and the protein precursor. (**b**) In volume, protein cross-linking occurs in the laser focus along the writing path in the protein precursor material. Diameter and height of volume elements, so-called voxel, in a free space become ellipsoidal shapes due to mismatch between focused spot sizes and Rayleigh length, as indicated by dashed and solid lines. On the substrate, surface bound structures are formed, depending on the position of focus. Determining resolution as the smallest distance between distinguishable structures, well-connected 3D structures can be formed by scanning the focused laser beam with a step smaller than the resolution. The box inset shows that protein molecules (light blue) in the precursor are interacted with photoactivator (orange) to be cross-linked (dark blue). The circular inset shows an SEM image of an icosahedron with submicron feature sizes, scale bar represents 1 μm, reprinted from ref. [33], with the permission of AIP Publishing, copyright 2015.

galvano scanning or DMD projection techniques, different exposure doses or scanning speeds were chosen to adjust for the respective technique.

Solvents

The aqueous systems used in these processes typically are buffered solutions or commercially available protein stabilizing solutions. Organic solvents have also been reported, although these solvents could potentially modify the original tertiary structure of the protein and thereby its functionality could be impaired prior to fabrication. The addition of dimethyl sulfoxide (DMSO) has been shown to improve both viscosity and feature sizes[34], although higher concentrations of DMSO in the system can also affect the tertiary structure or even denature the protein[66]. It is unclear why DMSO improves feature sizes and fabrication quality, although the heat and electron transfer properties of this solvent might play a role, in addition to the attendant increase in the viscosity of the precursor solution. In order to mimic these features, a glycerol-water solvent was employed in a prior work[37]. Because high concentrations of glycerol can be used to preserve proteins[71], this solvent does not risk damaging the protein at any concentration. When fabricating in glass microfluidic channels, light refraction and aberration due to refractive index changes between device and protein precursor material caused an increase in feature sizes and limited penetration depth[37]. Use of glycerol-water solvents provided an improved refractive index match to glass with n=1.51 from pure water n=1.333 to

over n=1.398, resulting in nearly unchanged feature sizes[37]. Additional investigations of refractive index matching and viscosity optimization in conjunction with proteins could allow glycerol-water solvents to be used to refine the fabrication process[72].

Photoactivator systems

Photoactivator involves molecules of either photoinitiator or photosensitizer that upon light absorption undergo reaction to create a reactive species or a chemical change in another molecule, respectively. The reactive species or the chemical change is relevant in the subsequent light-independent processes, here cross-linking. The efficiency of photoactivator is defined as the ratio of activated molecules, here cross-linked molecules after initiation, to all available molecules. The higher efficiency allows faster scanning speeds applicable during fabrication. The efficiency depends on the light absorption properties as well as the number of reactive species generated by the photoactivator.

Classical biological dyes, including MB, RB, rhodamine and eosin-y, are typically used to demonstrate fabrication principles and to understand the cross-linking mechanism. These dyes are known for their good absorption properties and their ability to generate radicals. Conjugated dyes such as Texas Red and fluorescein isothiocyanate (FITC) have high absorption coefficients and also enhance cross-linking.

There have been on-going attempts to identify efficient photoinitiators to allow the industrialization of polymer cross-linking and 3D printing. The use of effective photoinitiators could improve the fabrication process and also expand the range of applicable proteins. As an example, a benzophenone derivative (BPD) was used to cross-link small amounts of various types of collagen[52], while the water-soluble compound sodium 4-[2-(4-morpholino)benzoyl-2-dimethylamino]butylbenzenesulfonate (MBS) was utilized to cross-link enhanced green fluorescent protein (EGFP)[37]. A three-component system comprising a protein, rhodamine B and flavin adenine dinucleotide (FAD) significantly improved both fabrication speed and feature sizes[66]. However, additional increases in efficiency could increase the risk of generating radicals that would lead to cytotoxicity during the fabrication, as well as chemical leaching that is undesirable in various applications.

Due to their long triplet state lifetimes, with moderate radical generation, FAD and flavin mononucleotide (FMN) have been used for *in situ* cell applications over short time spans[56]. Several studies involving low photoinitiator concentrations have demonstrated that the threshold protein concentration required for fabrication increases dramatically[32,33,68]. Fabrication without photoinitiators has also been reported[32,33,49,68], although some attempts were unsuccessful[48]. Such discrepancies in prior works indicate that controlling all the major factors such as laser properties, irradiation conditions, solvent, photoactivator and protein concentration that can affect the outcome of the process is the key to achieving repeatability.

Proteins

High concentrations of protein precursor materials (which are discussed in more detail in Section: Structures and functions of cross-linked proteins) are required for cross-linking. These high concentrations are best achieved by dispersing the required amount of protein powder in a small solvent volume, following by stirring or shaking for a prolonged time period to ensure complete mixing. Even at elevated concentrations of 400 or 600 mg/mL in conjunction with a relatively large amount of a photoinitiator, fabrication appears to be possible only when applying a slower scanning speed relative to that used during polymer cross-linking. Low concentrations of proteins still allow for cross-linking but increase the fabrication threshold and require the use of higher photoinitiator concentrations[33]. Phragma dialysis can increase protein concentrations, but can only be applied for several repetitions due to the physical take-off volume limit. An alternative demonstrated by several groups involves mixing bovine serum albumin (BSA) with other proteins to retain the function of these other proteins while inducing cross-linking[32,38,43,56].

The protein concentration also significantly affects various irradiation parameters, in particular the penetration depth of the laser beam. Protein solutions may appear slightly colored, but are still transparent. Higher protein concentrations inevitably lead to greater beam absorption and scattering at shallower penetration depths. Cross-linking at deeper regions can be accomplished by controlling the laser light dose applied, although the protein cross-linking is quickly saturated at the surface. In addition, the aqueous protein solutions described above can be sensitive to the heat generated at higher laser powers. Unfortunately, the already low scanning velocities cannot be further reduced while retaining practical fabrication processes.

Proteinaceous microstructures have been found to have relatively low Young's modulus values in the range of 0.5–4 MPa[43,45,63], leading to poor mechanical stability that makes it difficult handle and preserve these structures. There are two established means of obtaining protein-polymer hybrid structures that combine the mechanical strength and chemical inertness of the polymer with the functionality of the protein. One approach is to conjugate the protein with acrylate, allowing the polymer chemistry to govern the cross-linking process[44]. This procedure has been successful employed with high molecular weight cellular matrix proteins such as collagen. The other approach uses protein-polymer adhesion after sufficient roughening of the polymer surface, such that the native protein does not undergo chemical changes[43].

Structures and functions of cross-linked proteins

In this section, the protein properties that are necessary for cross-linking are discussed based on representative proteins chosen from the protein data bank (PDB)[73], as indicated in Table 1. The role of BSA as a standard material and the function retention of cross-linked proteins are also addressed.

PDB

When considering cross-linking, it is important to understand where and how the cross-linking takes place, as this enables us to chemically control the microstructure growth of modified or artificial proteins. Figure 2 shows the secondary structures, unique chains, chain lengths, total unit weights and amino acid counts within the protein sequences of 16 different protein structures, all obtained from selected PDB data files. These properties reflect protein tertiary structure, stereo-accessibility, and potential sensitivity for cross-linking processes.

Secondary structure features such as alpha-helices, beta-sheets and unassigned parts are associated with certain groups of amino acids, but also give rise to stereo-accessibility or lack thereof. Figure 2a shows that there is no clear trend amongst these proteins. In order to connect ordered secondary structures, a protein always has some unassigned, likely unstructured regions and so it is not surprising to find approximately 50% unassigned chains. Among this small selection of proteins, the two proteins 3HQV and 3GHG have considerably more unassigned sequence parts while proteins 4F5S, 2CMM and 1OCC have relatively few unassigned sequence parts. There also seems to be no trend regarding alpha-helices and beta-sheets that would be beneficial for cross-linking.

The number of unique chains, so-called subunits, is

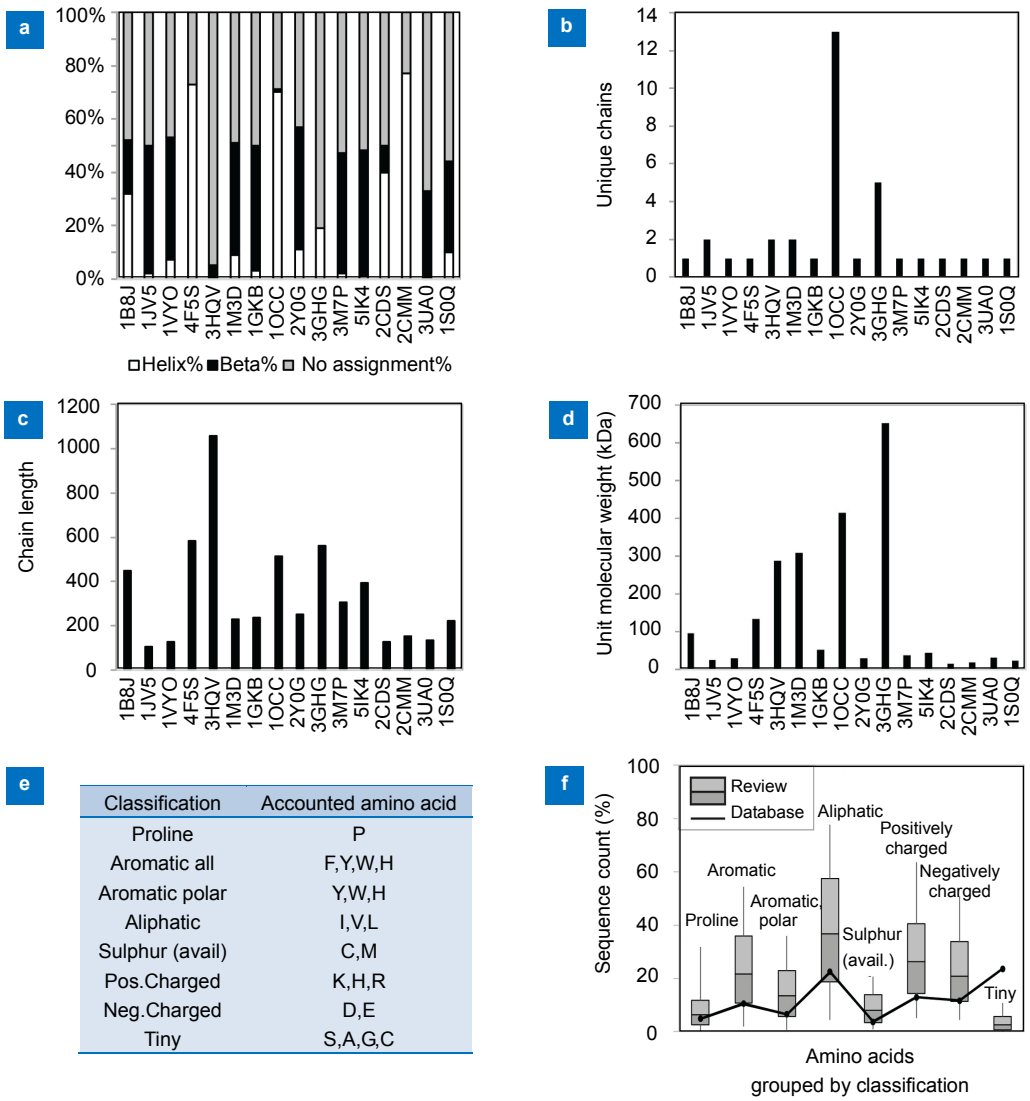

Classification	Accounted amino acid
Proline	P
Aromatic all	F,Y,W,H
Aromatic polar	Y,W,H
Aliphatic	I,V,L
Sulphur (avail)	C,M
Pos.Charged	K,H,R
Neg.Charged	D,E
Tiny	S,A,G,C

Fig. 2 | PDB data overview. Properties of 16 different protein structures obtained from selected PDB files: (**a**) the secondary structures, (**b**) unique chains, (**c**) chain lengths, (**d**) unit weights, and (**e**)–(**f**) amino acid distributions. (**e**) Single letter amino acid codes sorted by classification according to Livingstone et al. from ref. [74]. (**f**) The distributions of amino acid occurrence in the PDB FASTA sequence for 16 proteins versus respective database values, calculated from reports by Eitner et al. from ref. [75].

depicted in Fig. 2b. This value indicates how many chains may not be covalently bound, although other forces may lead to interactions between the chains that constitute the proteins used to acquire the PDB data. It is evident that most have one unique chain. This trend is expected since non-covalently bound protein chains might not be fully included in the cross-linking and thus tend to render the tertiary structure of the protein incomplete and disrupted. Interestingly, there is also one extreme example of successful protein cross-linking with cytochrome C, where 13 unique majorly helical chains interact to form the protein. It would be challenging to cross-link proteins that have associated metal units, but the 13 unique chains of cytochrome C suggest that even fabrication of complex proteins might succeed. In fact, Connell et al. reported the successful cross-linking of myoglobin, which binds iron via porphine in a similar manner to the red blood cell protein hemoglobin[47]. It is unclear whether appropriate iron was available during the fabrication or if iron porphine was associated throughout the process in the prior work, but it is likely that supplying the appropriate quantity of iron porphine after fabrication would lead to reconstituting iron complexes in the proteinaceous microstructure.

Protein chain lengths and weights are summarized in Figs. 2c and 2d, which also show no clear trend in terms of length, weight or the ratio of these two factors. It was previously assumed that, in general, molecular weight affects cross-linking and higher weights should result in a lower fabrication threshold. Pitts et al. provided results comparing fibrinogen with BSA[32] and showed that, although the molecular weight of fibrinogen is much higher than that of BSA, only at low photoinitiator concentration fibrinogen cross-linking occurred 2–10 times faster. This observation demonstrates that molecular weight is not necessarily an important factor. It is probable that stereo-accessibility and amino acid presentation are more important to successful cross-linking.

Figures 2e and 2f can be used to determine differences in the amino acid distributions of the 16 different proteins, based on the amino acid counts reported by Eitner et al.[75] In order to reasonably summarize the amino acids from individual counts, we followed the amino acid classification suggested by Livingstone et al.[74] The classifications and respective counts of amino acids are shown as single letter codes in Fig. 2e. These same single letter codes are also used to describe the FASTA protein sequences in the PDB. Counting the single letter codes within all sequences results in the distributions represented by the box plot graphs in Fig. 2f. The amino acid counts within the entire database were obtained from ref.[75] and are summarized by the same classifications. The results demonstrate that the proline distribution is quite similar to the database value. It should be noted that the proline content of Col. I is significantly different from the median and contributes to the broadening of the distribution. Possibly, with more reports of cross-linked proteins, the distribution might align fully with that of proline. In addition, all aromatic amino acids, aliphatic amino acids, amino acids with accessible sulfur residues (with S (serin) excluded), and positively and negatively charged amino acids score higher than the database values by about a quartile of their distributions. Again, this result could still change with more cross-linked protein entries. It is, however, interesting to note that amino acids with residues that could undergo radical or ion chain reactions score higher. This higher availability might hint at the protein cross-linking mechanism(s). Finally, so-called tiny amino acids that are not expected to contribute to any potential cross-linking mechanism show significantly higher counts in the general database and even lie outside of the distribution of the cross-linked proteins. Scanning the protein sequence for notably higher amino acid counts disregards the importance of stereo-accessibility, but could provide some initial insights into relevant amino acids.

Retention of protein function

One or several functions of a protein are generated by an active functional domain in the protein structure. As far as currently understood, the cross-linking process is random, it can affect the functional domain of a protein such that the individual protein molecules lose their function. However, written submicron-sized lines of protein would consist of many individual protein molecules which could still retain some function on a statistical basis. Therefore, the retention of function also depends on the type of protein and robustness in response to changes in or near the functional domains.

Figure 3 illustrates a fictive example comparing laser induced cross-linking and surface adhesion for biological applications of cell adhesion[43]. When a protein adheres to a surface, depending on the surface charges and potentials, the protein can lose function due to structural deformation or simply because the functional domains are rendered inaccessible. Figure 3a shows a protein with a functional domain, and Fig. 3b illustrates the manner in which potential conformational changes affect the function retention of that domain. Understanding that a conformational change can either significantly inhibit functioning or still allow full activity, direct laser writing processes are compared with surface adhesion in Figs. 3c and 3d. Direct laser writing is assumed to be a randomized process in which some molecules undergo large conformational changes while others undergo only minimal changes. Using cell adhesion to the protein as an example, the grey arrows demonstrate that some parts of the direct laser write-fabricated element repel the cells because the protein function is impaired, while other areas support cell adhesion because function is retained. In the case of the surface adhesion of the protein to four different surfaces, the surface charge and potential lead to more highly

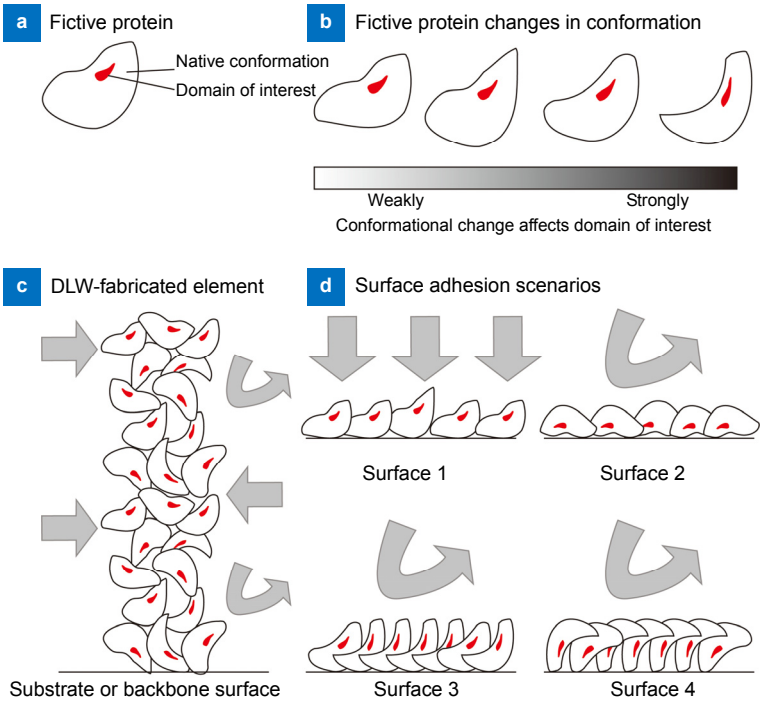

Fig. 3 | Proposed processes for protein cross-linking and adherence. A schematic illustration depicting the differing degrees of deformation and adhesion that can degenerate protein functionality. Specific surfaces render the functional domain inaccessible or can have little effect on the native protein, leading to retained protein function. Figure reprinted with permission from supplementary material of ref. [43], copyright 2017, American Chemical Society.

organized structures in which the functionality is either completely retained (surface 1) or completely impaired (surfaces 2–4), depending on the extent to which the surface potential of the protein leads to adhesion. This figure demonstrates the manner in which the randomness of the cross-linking process makes the fabricated element more likely to retain the protein function.

There have been various reports documenting the retention of binding function. Kaehr et al. showed that binding fluorescence is proportional to the protein concentration[56], implying not only retained function but also a non-preferential process. There have also been some reports about the retention of protein enzymatic functions[35,36,38]. However, to date there have been no analyses of protein activity or quantitative assessments of active units. It would be challenging to actually perform such experimentation, since the surface area and availability of the protein can affect the results, thus differences between bulk and laser-fabricated samples could be important.

Biodegradation of these materials has also been unexplored. Assuming that the cross-linking proceeds as a random process, one would expect that the resulting structures would be degradable because the majority of normal peptide or organic bonds would be retained. Sun et al. showed changes in proteinaceous structures within two weeks of exposure to collected raindrops, such that the surface became rougher, small features were reduced and structural elements seemed less supportive[41]. These observations suggested that complete degradation could occur within several months, although this was not confirmed.

Bovine serum albumin as a common standard

Table 1 confirms that almost all prior studies utilized bovine serum albumin (BSA). Figure 2 demonstrates that BSA (4F5S) consists primarily of alpha-helix components and that the molecular weight and height of this material match the common average values of the current protein group. Additionally, BSA is an affordable, abundant blood serum protein, and is a good representative of the average properties of such materials[76].

BSA also exhibits several other interesting properties as a blood regulating protein. Because BSA is found in blood, in which clotting is undesirable, BSA does not show specific binding preferences, although it will undergo non-specific binding to surfaces such as other proteins. Harper et al. noted that BSA was also selected in their work as a protein monomer due to its oxygen radical scavenger functionality[57].

Because of its availability and previous reports, BSA fabrication parameters have been well studied. It allows to become a standard to introduce and discuss variation of the major factors including laser properties, irradiation conditions, solvent, photoactivator and protein concentration, that can affect the outcome of the process. BSA is also often used due to its unique properties, one of which is pH actuation capability[39,40,62], as discussed later. Kaehr et al. have also shown its potential to be mixed with other

proteins and create a binding gradient that reflects the retained function of other proteins[39].

Cross-linking mechanisms

The cross-linking mechanisms associated with these techniques are not yet fully understood, although we can discuss various key aspects of these mechanisms. In the field of polymer science, multiple-step photo-induced reaction mechanisms are readily available to explain the growth dynamics of cross-linking. In the case of acidic pathways, organic monomers become acidic upon photo-excitation and interact with an aqueous base developer, while during hydrosilylation platinum colloids act as a catalyst after UV decomposition. In the case of radical chain reactions, radicals are generated by light irradiation and subsequently promote cross-linking while being regenerated.

Radical chain reactions involve unique dynamics due to the propagation and termination phases, which differ from both the acidic and catalytic mechanisms. Radical mechanisms tend to exhibit increased fabrication rates and can provide specific polymerization morphologies. This technique is commonly used for polymer cross-linking and has also been investigated as a possible mechanism for protein cross-linking. As a side note, one should keep in mind that the cross-linking of specific proteins with varying tertiary structural features could follow other mechanisms, including acidic mechanisms. These alternate mechanisms could involve acidic amino acids such as glutamate and aspartate or catalytic mechanisms based on metals such as iron or manganese as co-factors associated with the protein complex.

A radical chain reaction consists of three steps. The first is initiation, in which radicals are generated via irradiation. Propagation follows, during which radicals are generated simultaneous with growth of the polymer via interactions between radicals and monomers. Finally, termination occurs when radicals react with one another or with other compounds. Free radical initiated cross-linking reactions are typically exothermic[79].

Radical chain reactions in proteins

Spikes et al. used bulk poly-tyrosine and a photoinitiator to thoroughly investigate the interactions that follow light excitation[26]. The resulting hypothesis regarding this particular amino acid and a long-lived triplet state photoinitiator is summarized in Fig. 4a. Here, the carboxylic acid group of tyrosine undergoes photo-oxidation to generate a radical residue that subsequently forms a covalent bond between molecules. The nature of this covalent bond is not specifically known (for example: C-C, C-O-C or C-O-O-C). It is likely that various covalent bonds are formed with different probabilities correlating with their bonding strengths.

The ability to undergo photo-oxidation, including the ability of generating a radical from the carboxyl group, is associated with the amino acids cysteine, histidine, tyrosine, tryptophan and methionine[80,81]. Tyrosine, tryptophan and histidine are aromatic amino acids having a C-ring structure, while methionine and cysteine contain sulfur and thus contribute to disulfide bonds during the formation of the protein's tertiary structure. Cysteine residues have been thought to protect against oxidative damage, which hints at a sensitivity to photo-oxidation[82].

Pitts et al. pointed out that a photoinitiator that interacts with a coinitiator such as RB with triethanolamine (TEA) could cause an additional radical generation reaction[32], as shown in Fig. 4b. This reaction could enhance the occurrence of cross-linking due to higher radical concentrations, although this assumes radical formation in the protein molecules. It was also noted that protein itself might fulfill the role of co-initiator as well as crosslinkable species.

Protein cross-linking by DNA-bound metals has been investigated because protein-DNA cross-linking is used in cell analysis and *in situ* cell surgery[28]. As shown in Fig. 4c,

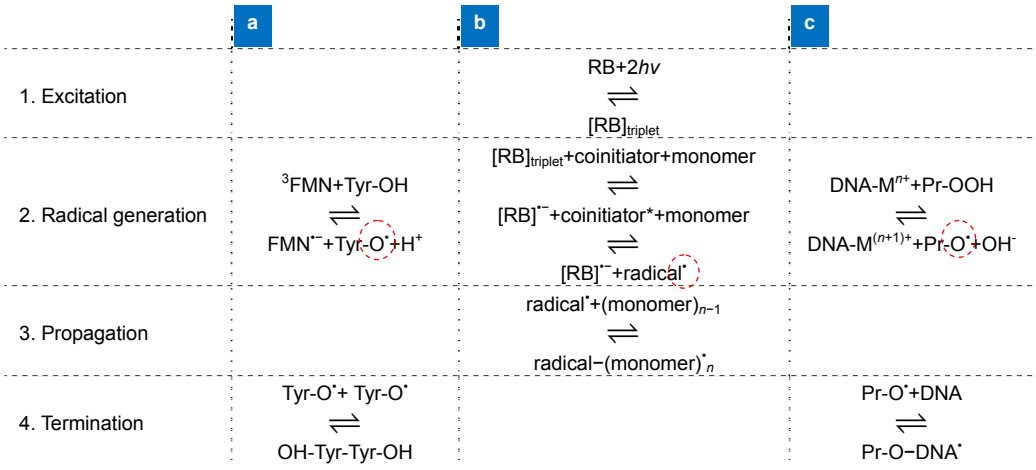

Fig. 4 | Proposed free radical mechanisms. Three selected protein cross-linking fabrication mechanisms based on radical oxygen formation inside the protein from (**a**) ref. [26], (**b**) ref. [32], and (**c**) ref. [28] are matched the four stages of light-induced radical chain reaction: excitation, radical generation, propagation and termination. Tyr represents tyrosine and M represents DNA-bound metal.

DNA is thought to initiate the reaction. Radical generation at the carboxyl group of the protein is proposed, leading to a C-O-DNA covalent bond.

When protein cross-linking has been attempted with little to no photoinitiator, the results have shown that the threshold dose for fabrication is increased. However, some attempts at photoinitiator-free fabrication have been unsuccessful, and so the mechanism of photoexcitation within a pure protein system must be explained. Potentially, aromatic amino acids (tyrosine, phenylalanine, tryptophan, histidine) and amino acids with a C-ring (proline) could undergo photo-excitation, either by promotion to an excited state (similar to FMN/FAD) or via the formation of radicals from carboxyl groups if these are available. In the case of proteins that are rich in negatively or positively charged amino acids, an ionic chain reaction could also be considered for the mechanism, although protein surface charges and surrounding water molecules might inhibit this reaction more so than the radical reactions.

The protein cross-linking mechanism evidently requires much more research both with and without a photoinitiator, and such studies could yield different results depending on the relevant amino acids.

Applications of proteinaceous microstructures

Due to the vast number of native and artificially engineered proteins, the potential for applications seems limitless. Current applications depend on either pH-actuation and soft optics, in which proteins are manipulated as deformable materials, or cell culture and microfluidics, where protein functions are harnessed. Enzymatic reactors have been developed to demonstrate this concept, and by choosing an applicable enzyme microfluidic enzymatic reactors might become important. Although no drug delivery applications have yet been reported, binding affinities could be utilized for enhanced recognition, as required in targeted delivery, or reduced recognition, such to reduce immune responses. In the near-future the retained functions of proteins could contribute to disease treatment or to the bottom-up rebuild of structures impacted by disease.

pH actuation

pH actuation is based on the swelling and shrinkage of cross-linked proteins[39] in response to environmental pH or salt concentration changes. Kaehr et al. showed that the swelling or shrinkage of different proteins occurs at different pH values, specifically that avidin swells at pH values that cause BSA to shrink, possibly as a result of their different isoelectric points[39]. It has also been reported that ionic strength variations can be used for actuation[39]. These findings suggest that swelling is associated with solvent interactions at the charged surface of the protein, which are translated to the overall proteinaceous microstructure.

In order to utilize chemical responsiveness, swelling and skeletal regions can be constructed in one structure made of a single protein but using different cross-linking densities[62], as shown in Fig. 5a. The cross-linking density can be changed by varying the pitch between fabrication layers, or possibly by varying the exposure dose.

This phenomenon has been applied to fabricate a mesh with tunable porosity (Fig. 5b)[62], a gripper-shaped actuator (Fig. 5c)[40] and pH-tunable lenses (Fig. 5d)[55]. In the latter, surface smoothness was important to achieving sufficient light transmission[55]. With regard to the actuator and mesh, unwanted contact and adhesion between the swollen material might make it difficult to use such devices in some applications. As well, swollen structures are even less mechanically robust than those in standard proteinaceous structures, which restricts potential mechanical applications. The mechanical strength could be increased by using polymer-protein hybrid structures[43] or higher cross-linking densities[44].

Soft microoptics

Using protein as a construction material for microoptics is a good option for the formation of environmentally friendly devices, because proteins are both renewable and degradable. In addition to the pH-tunable microlenses introduced in the previous section, a flexible micro-sized kinoform phase lens (KPL)[41] and a responsive whispering-gallery-mode micro-laser[53] have been fabricated based on this concept.

Figure 6a presents a KPL formed from polydimethylsiloxane (PDMS) as a flexible diffractive device with good surface properties and a suitable lifetime in an aqueous environment[41]. Three important aspects of this device are its quality, flexibility and capacity for biodegradation. This technique may therefore play an important role in the near future in terms of producing flexible, stretchable photonics and optics with a minimal environmental impact.

The concept of environmentally friendly optical devices[41,42] has also been demonstrated by the fabrication of a whispering-gallery-mode micro-laser[53]. Figure 6b shows the smoothness and fabrication accuracy of the disk structure that is necessary to control the gallery-mode. This micro-laser performed well in air as well as in aqueous solutions. Furthermore, Sun et al. demonstrated that the device was responsive to the ionic strength of the solution, thus suggesting applications in smart microfluidic devices[53].

Cell culture, *in situ* guidance and capture

Cell culture offers possibly the widest range of applications for proteinaceous microstructures due to the variety of cell-cell interactions and microenvironmental niches of cells. This field is divided into two aspects: continuous cultivation on scaffolds where the protein provides the microenvironment, and live interactions with *in situ* guidance or even capture of live cells.

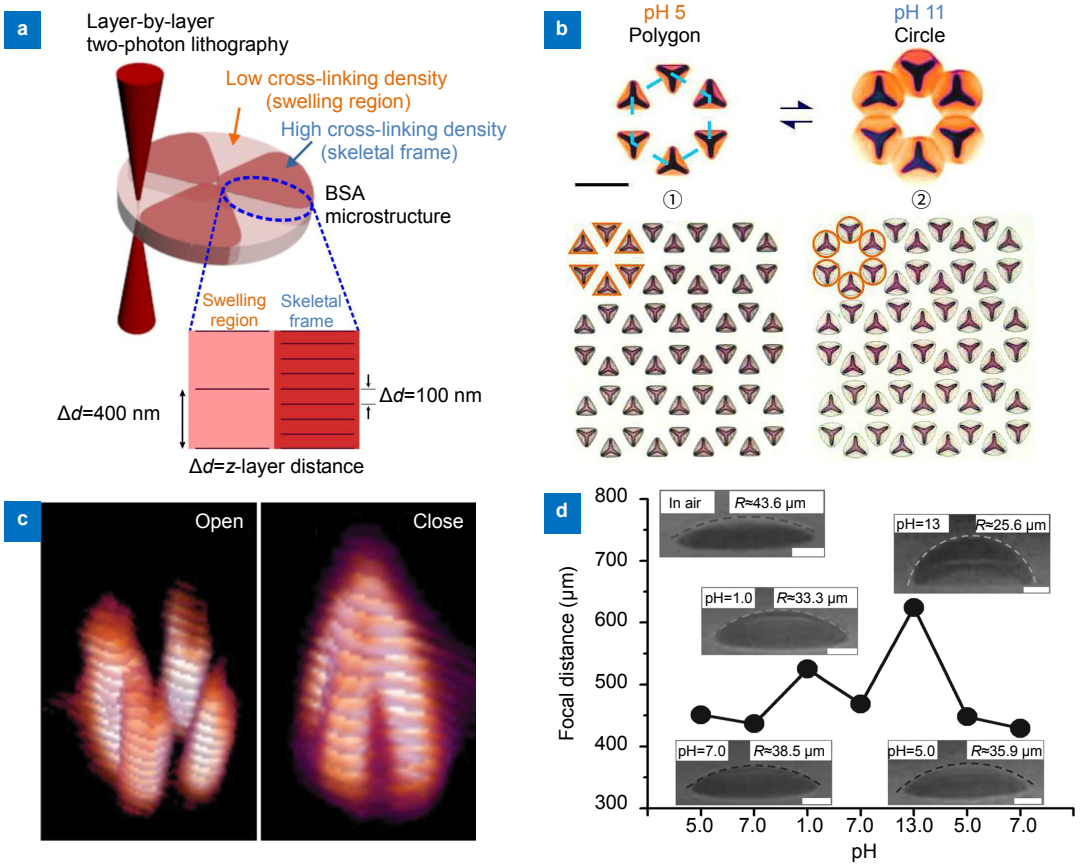

Fig. 5 | pH actuation. (**a**) Conceptual drawing of the fabrication of a device with regions having varying swelling properties in a protein solution in response to the same laser exposure. (**b**) Lay et al. designed a mesh pattern in which the porosity changes with pH. (**c**) pH-actuation of a microgripper, in which each pillar is approximately 5 μm wide at the base. (**d**) Dependence of the focal distance of a pH-tunable lens on pH. (**a**, **b**) Reprinted with permission from ref. [62], copyright 2015, American Chemical Society. (**c**) Reprinted with permission from ref. [40], copyright 2015, John Wiley and Sons. (**d**) Reprinted with permission from ref. [55], copyright 2015, John Wiley and Sons.

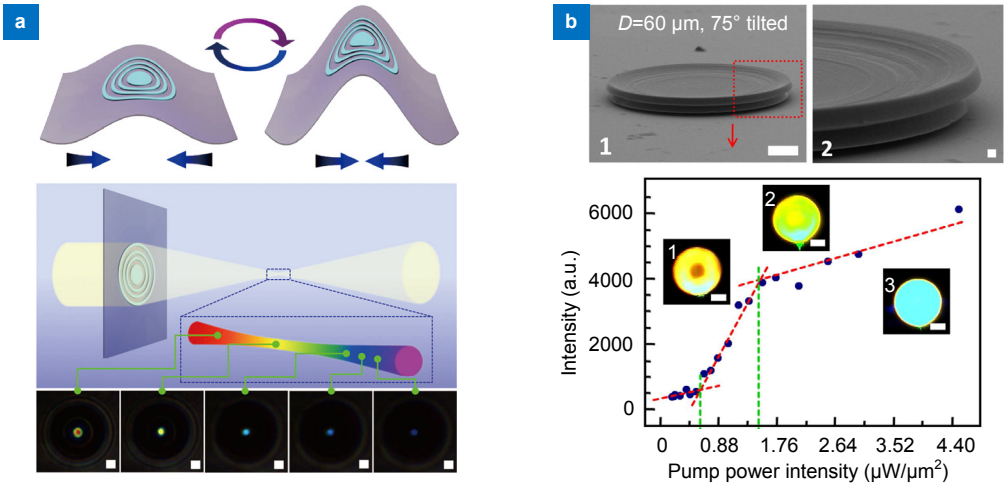

Fig. 6 | Soft microoptics. (**a**) A schematic illustration of the repetitive bending of KPL made of protein formed on a PDMS sheet (upper), and light diffraction results at different positions along the main light axis (lower). (**b**) A stimulus-responsive whispering-gallery-mode micro-laser fabricated from BSA. This structure requires high accuracy in fabrication and performs in air (shown) and aqueous environments. (**a**) Adapted by permission from Springer Nature: *Light Sci. Appl.*[41], copyright 2014. (**b**) Adapted by permission from Springer Nature: *Sci. Rep.*[53], copyright 2015.

Reports of cell culture scaffolds have focused on utilizing proteins to promote cell adhesion, with the specific protein dependent on the cell type, and including collagen type I, type II, type IV, fibronectin and BSA mixtures with such proteins[43,44,48,50,52,59,66,67]. Figures 7a and 7b show two recent examples of 3D cell culture scaffolds composed of at least two different materials that control cells spatially via adhesion. Using a protein scaffold composed

of BSA and fibronectin with broader feature sizes are typically available from direct laser writing (Fig. 7a), Da Sie et al. demonstrated that cell migration varied on different proteinaceous scaffold areas[60]. Fine, complicated networks created from complex solutions containing collagen type IV were embedded into polymer frames (Fig. 7b), confirming cell adhesion to these networks, as well as the formation of neurite-like extensions and interactions with individual network elements[43].

A much more challenging task is the live guidance or *in situ* capture of cells. Harper et al. used DMD-controlled layer-by-layer fabrication of a chamber to capture individual bacterial cells, as shown in Fig. 7c[57]. This level of isolation allowed single cell analysis to be performed, with the cells continuously incubated to study their progeny after single cell capture. When cells are robust against pH changes, pH-actuation can also be applied to release entrapped bacterial cells from a specifically designed trap structure[39]. Using a protein solution based on FAD with short application times, Kaehr et al. showed that direct free line writing allowed confining the growth of a neuronal cell in 2D[56], as can be seen from Fig. 7d.

Microfluidics

Microfluidic devices provide a small footprint, high sensitivity, diverse features and compartmentalization for biological studies because of their micro-sized structures composed of channels and chambers[83]. By integrating appropriate functions into channels or chambers, microfluidic devices can amongst others allow drug screening based on bodily functions using organ- or body-on-a-chip devices[84], as well as complex diagnostics by lab-on-a-chip or micro total analysis systems (μ-TAS)[85]. Integration of desired functions in specific regions within the glass or polymer microfluidic device enhances the device versatility and complexity.

As discussed in previous sections, cross-linked proteins retain their functions. Enzymatic as well as cell adhesion properties have been clearly demonstrated. Figure 8 shows some examples of the integration of proteinaceous microstructures into PDMS and glass microfluidic devices in conjunction with suitable 3D structures at resolutions typical of those obtained from laser direct writing.

Utilizing the binding function of anti-A antibodies, Lin et al. fabricated structures to capture red blood cells in a PDMS channel, as shown in Fig. 8a[35]. Subsequent to the bonding of the PDMS to the glass substrate, simplified pad-like proteinaceous microstructures were fabricated after introducing the precursor solution by a syringe. A BSA pad microstructure remained without adhering red blood cells, demonstrating that anti-A antibody function was essential to the capture.

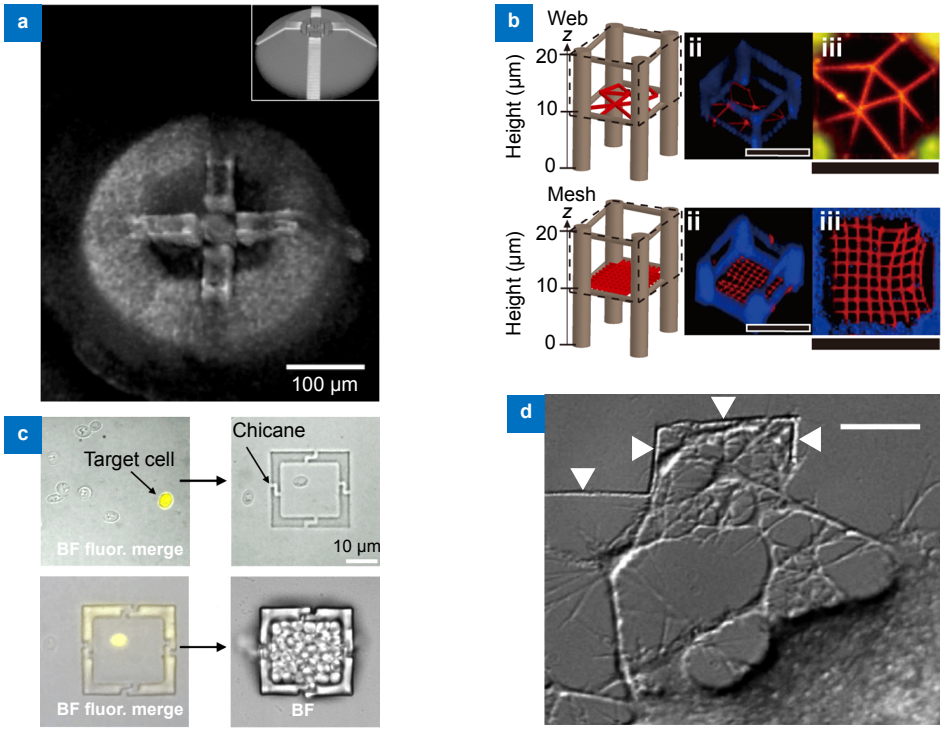

Fig. 7 | Cell culture scaffold and *in situ* guidance. (**a**) A two-protein microscaffold made with fibronectin and BSA to selectively cultivate cells only on the fibronecting elements. (**b**) Proteinaceous networks embedded in a mechanically supportive polymer scaffold to provide a microenvironment. (**c**) *In situ* observation of a captured bacterial cell with a fluorescent marker. The encapsulated bacterial cell had access to a nutritional medium and multiplied while trapped (scale bar represents 10 μm). (**d**) *In situ* guiding of neuronal cells by directly writing free lines (indicated by white arrows) near the cellular extensions (scale bar represents 10 μm). (**a**) Reprinted with permission from ref. [59], copyright 2015, OSA Publishing. (**b**) Reprinted with permission from ref. [43], copyright 2017, American Chemical Society. (**c**) Adapted with permission from ref. [57], copyright 2012, American Chemical Society. (**d**) Reprinted with permission from ref. [56], copyright 2004, National Academy of Sciences.

Iosin et al. integrated enzyme reactors into prefabricated PDMS channels, as shown in Fig. 8b[36]. However, the connectivity between the proteinaceous microstructures and PDMS channel ceiling and walls seemed incomplete and the ability of the proteinaceous microstructures to withstand the deformation of the flexible PDMS channel was not explored.

Figure 8c shows a proteinaceous microstructure integrated into closed glass microfluidics[37]. Such 3D glass microfluidics were first fabricated by femtosecond laser direct writing modification followed by thermal treatment and successive wet etching[86]. Using a glycerol-water solvent for the protein solution, the feature sizes in the closed microfluidic channel were as well-resolved as those on glass surfaces due to reduced refraction mismatch during the laser beam propagation. It was found to be possible to span a 3D design across the entire cross-section of the closed microchannel with a height of 20 μm. Preservation of dry 3D structures was challenging as they readily collapsed during the drying process or were torn apart when adhered to multiple glass channel walls due to the water volume loss. Figure 8c also presents the subsequent integration of EGFP and BSA proteins, demonstrating the potential versatility required for multi-protein applications.

Conclusion

The fabrication of 3D proteinaceous microstructures is an advancing field with great potential, due to the consequent retention of protein function and the availability of a vast range of different types of proteins. Similar to the field of polymer science, protein cross-linking is increasingly growing as a research subject. The associated mechanisms and the key protein properties that allow convenient fabrication have not yet been identified. However, even without this systematic understanding, some proteins have been utilized to execute specific applications.

The applications reported herein can be divided into two categories. One takes advantage of the deformability of proteins to obtain pH-activated devices and soft optics. The other uses binding affinities or enzymatic reactivities for cell culture and microfluidic integration. Furthermore, because binding affinity might induce swelling in response to molecules similar to the reported response to pH changes, a combination of both principles seems feasible. Protein cross-linking may also be a useful means of capturing live cells *in situ*. Combining protein functions with specific structural designs is expected to greatly expand the applications of this technique.

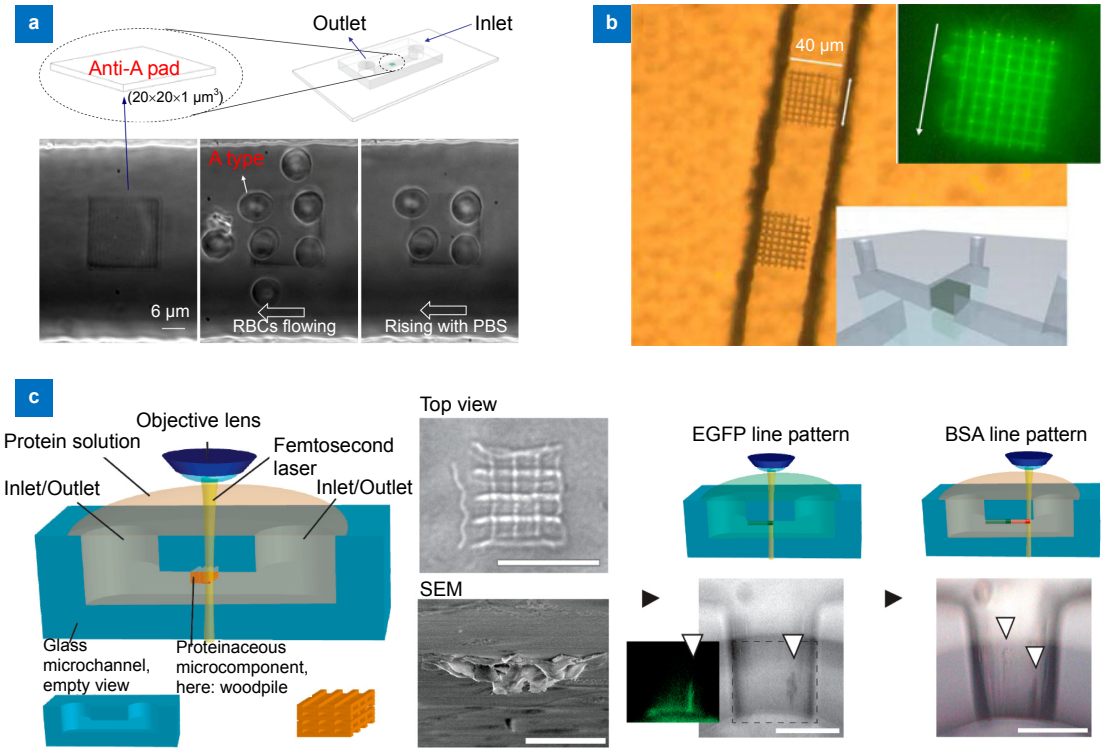

Fig. 8 | Microfluidic integration. Proteinaceous structures integrated into (**a**), (**b**) polydimethylsiloxane (PDMS) and (c) glass microfluidic devices. (**a**) Live capture of red blood cells (RBCs) based on type A binding to an anti-A antibody protein pad. (**b**) Enzyme reactors made from trypsin integrated into a PDMS channel. (**c**) Integration of BSA microstructures (top view during fabrication with 25 μm scale bar and SEM perspective view with 10 μm scale bar) and an EGFP pattern and BSA pattern in a closed glass microfluidic channel with 100 μm scale bars. (**a**) Reprinted by permission from the authors and SPIE [35], copyright 2015. (**b**) Adapted by permission from Springer Nature: *Microfluids and Nanofluids* [36], copyright 2011. (c) Adapted with permission from ref. [37], copyright 2018 MDPI.

References

1. Maskarinec S A, Tirrell D A. Protein engineering approaches to biomaterials design. *Curr Opin Biotechnol* **16**, 422–426 (2005).
2. Latour Jr R A. Biomaterials: protein–surface interactions. In Bowlin G L, Wnek G. *Encyclopedia of Biomaterials and Biomedical Engineering* 270 (Marcel Dekker, 2013).
3. Ruel-Gariépy E, Leroux J C. In situ-forming hydrogels—review of temperature-sensitive systems. *Eur J Pharm Biopharm* **58**, 409–426 (2004).
4. Teixeira L S M, Feijen J, van Blitterswijk C A, Dijkstra P J, Karperien M. Enzyme-catalyzed crosslinkable hydrogels: emerging strategies for tissue engineering. *Biomaterials* **33**, 1281–1290 (2012).
5. Shen W, Lammertink R G H, Sakata J K, Kornfield J A, Tirrell D A. Assembly of an artificial protein hydrogel through leucine zipper aggregation and disulfide bond formation. *Macromolecules* **38**, 3909–3916 (2005).
6. Williams R J, Hall T E, Glattauer V, White J, Pasic P J *et al*. The *in vivo* performance of an enzyme-assisted self-assembled peptide/protein hydrogel. *Biomaterials* **32**, 5304–5310 (2011).
7. Zubtsov D A, Ivanov S M, Rubina A Y, Dementieva E I, Chechetkin V R *et al*. Effect of mixing on reaction–diffusion kinetics for protein hydrogel-based microchips. *J Biotechnol* **122**, 16–27 (2006).
8. Wu J H, Li P F, Dong C L, Jiang H T, Xue B *et al*. Rationally designed synthetic protein hydrogels with predictable mechanical properties. *Nat Commun* **9**, 620 (2018).
9. Elzoghby A O, Samy W M, Elgindy N A. Protein-based nanocarriers as promising drug and gene delivery systems. *J Control Release* **161**, 38–49 (2012).
10. Kou S Z, Yang Z G, Sun F. Protein hydrogel microbeads for selective uranium mining from seawater. *ACS Appl Mater Interfaces* **9**, 2035–2039 (2017).
11. Onoe H, Okitsu T, Itou A, Kato-Negishi M, Gojo R *et al*. Metre-long cell-laden microfibres exhibit tissue morphologies and functions. *Nat Mater* **12**, 584–590 (2013).
12. Hsiao A Y, Okitsu T, Onoe H, Kiyosawa M, Teramae H *et al*. Smooth muscle-like tissue constructs with circumferentially oriented cells formed by the cell fiber technology. *PLoS One* **10**, e0119010 (2015).
13. Kato-Negishi M, Onoe H, Ito A, Takeuchi S. Rod-shaped neural units for aligned 3D neural network connection. *Adv Healthc Mater* **6**, 1700143 (2017).
14. Bahukudumbi P, Carson K H, Rice-Ficht A C, Andrews M J. On the diameter and size distributions of bovine serum albumin (BSA)-based microspheres. *J Microencapsul* **21**, 787–803 (2004).
15. Suslick K S, Grinstaff M W, Kolbeck K J, Wong M. Characterization of sonochemically prepared proteinaceous microspheres. *Ultrason Sonochem* **1**, S65-S68 (1994).
16. Silva R, Ferreira H, Vasconcelos A, Gomes A C, Cavaco-Paulo A. Sonochemical proteinaceous microspheres for wound healing. In Zahavy E, Ordentlich A, Yitzhaki S, Shafferman A. *Nano-Biotechnology for Biomedical and Diagnostic Research* 733 (Springer, 2012).
17. Forsberg F, Goldberg B B, Liu J B, Merton D A, Rawool N M. On the feasibility of real-time, in vivo harmonic imaging with proteinaceous microspheres. *Ultrasound* **15**, 853–860 (1996).
18. Boland T, Xu T, Damon B, Cui X F. Application of inkjet printing to tissue engineering. *Biotechnol J* **1**, 910–917 (2006).
19. Roth E A, Xu T, Das M, Gregory C, Hickman J J *et al*. Inkjet printing for high-throughput cell patterning. *Biomaterials* **25**, 3707–3715 (2004).
20. Geckil H, Xu F, Zhang X H, Moon S J, Utkan D. Engineering hydrogels as extracellular matrix mimics. *Nanomedicine* **5**, 469–484 (2010).
21. Kang H W, Lee S J, Ko I K, Kengla C, Yoo J J *et al*. A 3D bioprinting system to produce human-scale tissue constructs with structural integrity. *Nat Biotechnol* **34**, 312–319 (2016).
22. Delaporte P, Alloncle A P. Laser-induced forward transfer: a high resolution additive manufacturing technology. *Opt Laser Technol* **78**, 33–41 (2016).
23. Zergioti I, Karaiskou A, Papazoglou D G, Fotakis C, Kapsetaki M *et al*. Femtosecond laser microprinting of biomaterials. *Appl Phys Lett* **86**, 163902 (2005).
24. Hopp B, Smausz T, Kresz N, Barna N, Bor Z *et al*. Survival and proliferative ability of various living cell types after laser-induced forward transfer. *Tissue Eng* **11**, 1817–1823 (2005).
25. Kattamis N T, Purnick P E, Weiss R, Arnold C B. Thick film laser induced forward transfer for deposition of thermally and mechanically sensitive materials. *Appl Phys Lett* **91**, 171120 (2007).
26. Spikes J D, Shen H R, Kopečková P, Kopeček J. Photodynamic crosslinking of proteins. III. Kinetics of the FMN-and rose Bengal-sensitized photooxidation and intermolecular crosslinking of model tyrosine-containing N-(2-hydroxypropyl) methacrylamide copolymers. *Photochem Photobiol* **70**, 130–137 (1999).
27. Moss T, Dimitrov S I, Houde D. UV-laser crosslinking of proteins to DNA. *Methods* **11**, 225–234 (1997).
28. Gebicki S, Gebicki J M. Crosslinking of DNA and proteins induced by protein hydroperoxides. *Biochem J* **338**, 629–636 (1999).
29. Sugioka K, Cheng Y. Ultrafast lasers—reliable tools for advanced materials processing. *Light Sci Appl* **3**, e149 (2014).
30. Sugioka K, Cheng Y. Femtosecond laser three-dimensional micro- and nanofabrication. *Appl Phys Rev* **1**, 041303 (2014).
31. Fischer J, Wegener M. Three-dimensional optical laser lithography beyond the diffraction limit. *Laser Photon Rev* **7**, 22–44 (2013).
32. Pitts J D, Campagnola P J, Epling G A, Goodman S L. Submicron multiphoton free-form fabrication of proteins and polymers: studies of reaction efficiencies and applications in sustained release. *Macromolecules* **33**, 1514–1523 (2000).
33. Serien D, Takeuchi S. Fabrication of submicron proteinaceous structures by direct laser writing. *Appl Phys Lett* **107**, 013702 (2015).
34. Spivey E C, Ritschdorff E T, Connell J L, McLennon C A, Schmidt C E *et al*. Multiphoton lithography of unconstrained three-dimensional protein microstructures. *Adv Func Mater* **23**, 333–339 (2013).
35. Lin C L, Pan M J, Chen H W, Lin C K, Lin C F *et al*. Laser cross-linking protein captures for living cells on a biochip. *Proc SPIE* **9310**, 93100D (2015).
36. Iosin M, Scheul T, Nizak C, Stephan O, Astilean S *et al*. Laser microstructuration of three-dimensional enzyme reactors in microfluidic channels. *Microfluid Nanofluid* **10**, 685–690 (2011).
37. Serien D, Kawano H, Miyawaki A, Midorikawa K, Sugioka K. Femtosecond laser direct write integration of multi-protein patterns and 3D microstructures into 3D glass microfluidic devices. *Appl Sci* **8**, 147 (2018).
38. Basu S, Campagnola P J. Enzymatic activity of alkaline phos-

phatase inside protein and polymer structures fabricated via multiphoton excitation. *Biomacromolecules* **5**, 572–579 (2004).
39. Kaehr B, Shear J B. Multiphoton fabrication of chemically responsive protein hydrogels for microactuation. *Proc Natl Acad Sci USA* **105**, 8850–8854 (2008).
40. Lee M R, Phang I Y, Cui Y, Lee Y H, Ling X Y. Shape-shifting 3D protein microstructures with programmable directionality via quantitative nanoscale stiffness modulation. *Small* **11**, 740–748 (2015).
41. Sun Y L, Dong W F, Niu L G, Jiang T, Liu D X *et al*. Protein-based soft micro-optics fabricated by femtosecond laser direct writing. *Light Sci Appl* **3**, e129 (2014).
42. Sun S M, Sun Y L, Zheng B Y, Wang P, Hou Z S *et al*. Protein-based Y-junction optical micro-splitters with environment-stimulus-actuated adjustments. *Sens Actuators B Chem* **232**, 571–576 (2016).
43. Serien D, Takeuchi S. Multi-Component microscaffold with 3D spatially defined proteinaceous environment. *ACS Biomater Sci Eng* **3**, 487–494 (2017).
44. Engelhardt S, Hoch E, Borchers K, Meyer W, Krüger H *et al*. Fabrication of 2D protein microstructures and 3D polymer–protein hybrid microstructures by two-photon polymerization. *Biofabrication* **3**, 025003 (2011).
45. Khripin C Y, Brinker C J, Kaehr B. Mechanically tunable multiphoton fabricated protein hydrogels investigated using atomic force microscopy. *Soft Matter* **6**, 2842–2848 (2010).
46. Hill R T, Lyon J L, Allen R, Stevenson K J, Shear J B. Microfabrication of three-dimensional bioelectronic architectures. *J Am Chem Soc* **127**, 10707–10711 (2005).
47. Connell J L, Ritschdorff E T, Shear J B. Three-dimensional printing of photoresponsive biomaterials for control of bacterial microenvironments. *Anal Chem* **88**, 12264–12271 (2016).
48. Turunen S, Käpylä E, Terzaki K, Viitanen J, Fotakis C *et al*. Pico- and femtosecond laser-induced crosslinking of protein microstructures: evaluation of processability and bioactivity. *Biofabrication* **3**, 045002 (2011).
49. Kaehr B, Ertas N, Nielson R, Allen R, Hill R T *et al*. Direct-write fabrication of functional protein matrixes using a low-cost Q-switched laser. *Anal Chem* **78**, 3198–3202 (2006).
50. Iosin M, Stephan O, Astilean S, Duperray A, Baldeck P. Microstructuration of protein matrices by laser-induced photochemistry. *J Optoelectron Adv M* **9**, 716–720 (2007).
51. Basu S, Wolgemuth C W, Campagnola P J. Measurement of normal and anomalous diffusion of dyes within protein structures fabricated via multiphoton excited cross-linking. *Biomacromolecules* **5**, 2347–2357 (2004).
52. Basu S, Cunningham L P, Pins G D, Bush K A, Taboada R *et al*. Multiphoton excited fabrication of collagen matrixes cross-linked by a modified benzophenone dimer: bioactivity and enzymatic degradation. *Biomacromolecules* **6**, 1465–1474 (2005).
53. Sun Y L, Hou Z S, Sun S M, Zheng B Y, Ku J F *et al*. Protein-based three-dimensional whispering-gallery-mode micro-lasers with stimulus-responsiveness. *Sci Rep* **5**, 12852 (2015).
54. Lawson J L, Jenness N, Wilson S, Clark R L. Method of creating microscale prototypes using SLM based holographic lithography. *Proc SPIE* **8612**, 86120L (2013).
55. Sun Y L, Dong W F, Yang R Z, Meng X, Zhang L *et al*. Dynamically tunable protein microlenses. *Angew Chem Int Ed* **51**, 1558–1562 (2012).
56. Kaehr B, Allen R, Javier D J, Currie J, Shear J B. Guiding neuronal development with *in situ* microfabrication. *Proc Natl Acad Sci USA* **101**, 16104–16108 (2004).
57. Harper J C, Brozik S M, Brinker C J, Kaehr B. Biocompatible microfabrication of 3D isolation chambers for targeted confinement of individual cells and their progeny. *Anal Chem* **84**, 8985–8989 (2012).
58. Nielson R, Kaehr B, Shear J B. Microreplication and design of biological architectures using dynamic-mask multiphoton lithography. *Small* **5**, 120–125 (2009).
59. Da Sie Y, Li Y C, Chang N S, Campagnola P J, Chen S J. Fabrication of three-dimensional multi-protein microstructures for cell migration and adhesion enhancement. *Biomed Opt Express* **6**, 480–490 (2015).
60. Ritschdorff E T, Nielson R, Shear J B. Multi-focal multiphoton lithography. *Lab Chip* **12**, 867–871 (2012).
61. Allen R, Nielson R, Wise D D, Shear J B. Catalytic three-dimensional protein architectures. *Anal Chem* **77**, 5089–5095 (2005).
62. Lay C L, Lee M R, Lee H K, Phang I Y, Ling X Y. Transformative two-dimensional array configurations by geometrical shape-shifting protein microstructures. *ACS Nano* **9**, 9708–9717 (2015).
63. Lay C L, Lee Y H, Lee M R, Phang I Y, Ling X Y. Formulating an ideal protein photoresist for fabricating dynamic microstructures with high aspect ratios and uniform responsiveness. *ACS Appli Mater Interfaces* **8**, 8145–8153 (2016).
64. Hernandez D S, Ritschdorff E T, Seidlits S K, Schmidt C E, Shear J B. Functionalizing micro-3D-printed protein hydrogels for cell adhesion and patterning. *J Mater Chem B* **4**, 1818–1826 (2016).
65. Jenness N J, Hill R T, Hucknall A, Chilkoti A, Clark R L. A versatile diffractive maskless lithography for single-shot and serial microfabrication. *Opt Express* **18**, 11754–11762 (2010).
66. Serien D, Takeuchi S. Two-Photon direct laser writing for proteinaceous microstructures with additional sensitizer. *J Laser Micro/Nanoeng* **12**, 80–85 (2017).
67. Bell A, Kofron M, Nistor V. Multiphoton crosslinking for biocompatible 3D printing of type I collagen. *Biofabrication* **7**, 035007 (2015).
68. Lyon J L, Hill R T, Shear J B, Stevenson K J. Direct electrochemical and spectroscopic assessment of heme integrity in multiphoton photo-cross-linked cytochrome *c* structures. *Anal Chem* **79**, 2303–2311 (2007).
69. Basu S, Campagnola P J. Properties of crosslinked protein matrices for tissue engineering applications synthesized by multiphoton excitation. *J Biomed Mater Res A* **71A**, 359–368 (2004).
70. Sun Y L, Li Q, Sun S M, Huang J C, Zheng B Y *et al*. Aqueous multiphoton lithography with multifunctional silk-centred bio-resists. *Nat Commun* **6**, 8612 (2015).
71. Vagenende V, Yap M G S, Trout B L. Mechanisms of protein stabilization and prevention of protein aggregation by glycerol. *Biochemistry* **48**, 11084–11096 (2009).
72. Hand D B. The refractivity of protein solutions. *J Biol Chem* **108**, 703–707 (1935).
73. Burley S K, Berman H M, Christie C, Duarte J M, Feng Z et al. RCSB Protein Data Bank: Sustaining a living digital data resource that enables breakthroughs in scientific research and biomedical education. Protein Sci 27, 316-330 (2018).
74. Livingstone C D, Barton G J. Protein sequence alignments: a strategy for the hierarchical analysis of residue conservation. *Bioinformatics* **9**, 745–756 (1993).

75. Eitner K, Koch U, Gawęda T, Marciniak J. Statistical distribution of amino acid sequences: a proof of Darwinian evolution. *Bioinformatics* **26**, 2933–2935 (2010).
76. Peters T. Serum albumin. *Adv Clin Chem* **13**, 37–111 (1970).
77. Yu T, Ober C K, Kuebler S M, Zhou W, Marder S R *et al*. Chemically amplified positive resists for two-photon three-dimensional microfabrication. *Adv Mater* **15**, 517–521 (2003).
78. Coenjarts C A, Ober C K. Two-photon three-dimensional microfabrication of poly(dimethylsiloxane) elastomers. *Chem Mater* **16**, 5556–5558 (2004).
79. Oster G. Dye-sensitized photopolymerization. *Nature* **173**, 300–301 (1954).
80. Dubbelman T M A R, De Goeij A F P M, Van Steveninck J. Protoporphyrin-induced photodynamic effects on transport processes across the membrane of human erythrocytes. *Biochim Biophys Acta Biomembr* **595**, 133–139 (1980).
81. Shen H R, Spikes J D, Kopečková P, Kopeček J. Photodynamic crosslinking of proteins II. Photocrosslinking of a model protein-ribonuclease A. *J Photochem Photobiol B* **35**, 213–219 (1996).
82. Requejo R, Hurd T R, Costa N J, Murphy M P. Cysteine residues exposed on protein surfaces are the dominant intramitochondrial thiol and may protect against oxidative damage. *FEBS J* **277**, 1465–1480 (2010).
83. Sackmann E K, Fulton A L, Beebe D J. The present and future role of microfluidics in biomedical research. *Nature* **507**, 181–189 (2014).
84. Huh D, Torisawa Y S, Hamilton G A, Kim H J, Ingber D E. Microengineered physiological biomimicry: organs-on-Chips. *Lab Chip* **12**, 2156–2164 (2012).
85. Fan X D, White I M. Optofluidic microsystems for chemical and biological analysis. *Nat Photonics* **5**, 591–597 (2011).
86. Wu D, Wu S Z, Xu J, Niu L G, Midorikawa K *et al*. Hybrid femtosecond laser microfabrication to achieve true 3D glass/polymer composite biochips with multiscale features and high performance: the concept of ship-in-a-bottle biochip. *Laser Photon Rev* **8**, 458–467 (2014).

Acknowledgements

This work was partially supported by the RIKEN SPDR program. This work was partially supported by The Amada Foundation Research Grant (Jyuten-Kenkyu-Kaihatsu-Josei A).

Competing interests

The authors declare no competing financial interests.